OPEN ACCESS JOURNAL

BIOINTERFACE RESEARCH IN APPLIED CHEMISTRY

ORIGINAL ARTICLE

www.BiointerfaceResearch.com

ISSN 2069-5837

Volume 2, Issue 3, 2012, 339-349

Received: 29.05.2012 / Accepted: 13.06.2012 / Published on-line: 15.06.2012

Mineralization and particle growth kinetics of ZnO in the presence of gelatin

Johannes Baier[1]*, Robin Strumberger[1], Frank Berger [1], Petia Atanasova[1],
Udo Welzel[2], Joachim Bill[1]

ABSTRACT

We have investigated the mineralization of zinc oxide and the kinetics of formation of zinc oxide - gelatin composites in colloidal suspensions at temperatures between 30 °C and 45 °C. Particle growth was studied *in situ* using dynamic light scattering (DLS). The activation energy of particle growth was determined by kinetic analysis of the DLS data. We obtained an activation energy of $E_{A,g} = (9.6 \pm 2.4)$ kJ mol^{-1} in presence and an activation energy of $E_{A,ZnO} = (71.0 \pm 10)$ kJ mol^{-1} in absence of gelatin B 225. Furthermore, the precipitation process and the morphology of the occurring particles were analyzed applying diverse methods. The phase formation and the crystallite size were investigated by X-ray diffractometry (XRD). The morphology of the particles was studied by scanning electron microscopy (SEM), where spherical particles in absence of gelatin B 225 and plate-like particles in presence of gelatin were found. The combination of these analytical techniques allowed us to develop a model for describing the particle formation.

Keywords: *ZnO, gelatin, bio-inspired, mineralization, dynamic light scattering, DLS, kinetics*

1. INTRODUCTION

In the field of ceramic materials, zinc oxide (ZnO) plays an important role. It is mainly used as an additive to improve the mechanical properties of polymers, cement, paints, food and many more. But also the electrical and optical properties of ZnO gain the interest of research [1]. Thin transparent semiconducting films of ZnO can be used as electrode within liquid crystal displays, solar cells, LED and transistors [2-4]. The synthesis of ZnO can often be achieved only by energy- and cost-intensive processes. Therefore, it is essential to investigate new methods of material synthesis. A subject of current research is bio-inspired material synthesis of technical relevant materials based on biological mineralization processes. Developed by natural selection, biomineralization forms solids like bones, shells and teeth without wasting energy and material. The obtained composites consist of organic and inorganic components. The organic phase acts as a template for inorganic substances like calcium carbonate, hydroxyapatite and silica, whereby complex structures can grow [5]. Regarding the mechanism forming this type of biominerals nonclassical crystallization is discussed. This process occurs at low temperatures, ambient pressure and in aqueous solution. It is a particle-mediated crystallization pathway in which diverse interactions of a colloidal system lead to self-organization of primary particles [6]. According to this principle, Bauermann et al. synthesized hexagonal zinc oxide particles with gelatin as organic component in a buffered aqueous solution [7-9]. In principle, only two components are necessary for zinc oxide precipitation: a soluble zinc salt and a reagent, which shifts the pH in a region of supersaturation of zinc oxide. Organic molecules

---

[1] Institute for Materials Science, University of Stuttgart, Stuttgart
*Corresponding author e-mail address: ***baier@imw.uni-stuttgart.de***
[2] Max Planck Institute for Intelligent Systems, Stuttgart

are essential for bioinspired mineralization processes. They influence the structure and composition of the crystallization nuclei as well as the particle size, texture, habit and aggregation, and stability of intermediate phases [10]. Andeen et al. found that charged citrate ions specifically adsorb onto the ZnO (001) surface and drastically reduce the growth in the [001] direction [11]. Lipowski et al. studied the time evolution of the thermally activated mineralization of ZnO nanoparticles in a methanol solution in the presence of polyvinylpyrrolidone. In that investigation, amorphous needle-like organic/inorganic hybrid particles were observed. These intermediate particles act as a reservoir for zinc ions that are released during the crystallization process [12].

Dynamic light scattering (DLS), as an *in situ* technique, is a powerful method to explore the particle growth in the nanometer range and hence the nucleation and aggregation processes in colloidal systems. In several studies, DLS was applied to investigate the kinetics of zirconium sulfate precipitation [13], aggregation of macromolecular systems [14], cluster formation of biomolecules [15] and nucleation and growth of thaumatin crystals [16]. On the basis of these studies, we used this technique to investigate the temperature-dependent particle size development in our system. Furthermore, pH measurements, scanning electron microscopy (SEM) and X-ray diffractometry (XRD) were used to gain a comprehensive insight into the occurring processes of particle formation in presence of gelatin B 225.

2. EXPERIMENTAL SECTION

2.1. Preparation of solutions. The protein gelatin from bovine skin, type B, 225 Bloom ($M_w \approx 50000$ g mol^{-1}) was dissolved in an aqueous buffer solution of 30 mmol l^{-1} tris(hydroxymethyl)aminomethane (Trizma). The buffer solution was prepared by dissolving 1.842 g l^{-1} Trizma hydrochloride and 2.22 g l^{-1} Trizma base in deionized water to adjust pH 8. The reaction was started by adding $Zn(NO_3)_2$ solution to achieve final concentrations of 0.85 g l^{-1} gelatin B 225, 21.18 mmol l^{-1} Trizma and 5.88 mmol l^{-1} $Zn(NO_3)_2{\bullet}6H_2O$. The solutions were preheated to the respective reaction temperature between 30 °C and 45 °C. The synthesis was realized both in presence and absence of protein. In both cases Trizma buffer was used within solutions. In absence of gelatin the analyzed temperatures were 25 °C, 30 °C and 37 °C. The chemicals used are reagent grade from Sigma Aldrich.

2.2. Dynamic Light Scattering (DLS). Immediately after starting the reaction, a small amount of the stock solution was transferred into a cuvette (Satstedt No./REF 67.754) that was placed in the heated measurement chamber of the apparatus (Malvern Instruments Zetasizer 3000HS Advanced). The light source was a He-Ne laser with a wavelength of 633 nm. DLS technique allows measuring the hydrodynamic radius d_H of particles and the time-dependent fluctuation of the scattering intensity, where the exponential decaying of auto-correlation function involves the important information about the translational diffusion coefficient D of particles [17]. The correlation functions were recorded every 30 s and evaluated with the corresponding Software PCS v.1.52. Applying the Einstein-Stokes-equation and the Arrhenius-Andrade-relation [18], the reciprocal relation between the translational diffusion coefficient D and hydrodynamic diameter d_H allows us to determine an activation energy of the particle diffusion $E_{A,d}$ with equation (1):

$$D = \frac{kT}{3\pi\eta_0 d_H} \exp\left[-\frac{E_{A,d}}{RT}\right]$$

with k the Boltzmann constant, T the absolute temperature, η_0 is the viscosity of the medium and R the ideal gas constant.

The calculation of the activation energy $E_{A,d}$ can be realized by transferring the diffusion coefficients D of each particle size into a diagram, where $\ln[D/T]$ versus $1/T$ is plotted, which follows equation

(1). The slopes for each particle size are represented by a straight line, which are proportional to the activation energy of particle diffusion $E_{A,d}$.

2.3. Scanning Electron Microscopy (SEM). The morphology of the particles was investigated using a Zeiss DSM 982 Gemini electron microscope at 3 kV. After particular reaction times the reaction tube was immersed in liquid nitrogen until the included suspension was frozen to stop the reaction and to prevent further particle growth. After thawing, the particles were dried at 39 °C. In presence of gelatin the obtained samples were heated at 600 °C for 10 h in air with a heating rate of 10 K min^{-1} on a silicon wafer in order to expose the ZnO crystals. It is a simple method in which no disaggregation or sintering of the particles occurs [7,19]. In absence of gelatin B 225, the heat treatment has been omitted. Before being analyzed, all samples were sputtered with Pt/Pd.

2.4. X-ray diffraction (XRD). The particle preparation was realized as described for SEM. The applied diffractometer was a Philips X'Pert MPD with Bragg-Bretano geometry and a primary beam monochromator to select the $K_{\alpha 1}$ component of the employed copper radiation ($\lambda = 1.54056$ Å). For line-broadening analysis, the reflections with a sufficiently high peak-to-background ratio in the diffraction angle range between about 30° and 40° (pertaining to the ZnO (100), (002) and (101) reflections) were investigated. Peak-maximum positions, full widths at half maximum (FWHM), integral breadths and integrated intensities were determined by fitting Pearson VII functions to the measured diffraction lines. The line broadening was analysed on the basis of the single-line method by attributing Lorentzian line broadening to crystallite size and Gaussian line broadening to microstrain [20]. A correction for instrumental broadening was done on the basis of reference measurements employing a powder layer of LaB_6 (Standard Reference Material SRM 660a, National Institute of Standard and Technology NIST, Gaithersburg, USA) deposited by sedimentation on a zero-background specimen holder using a Voigt-function approach to subtract instrumental broadening [20]. To analyze the occurring phases during the reaction the material was not heated after removing out of the solution. The material was dried at room-temperature in an Ar-beam.

2.5. pH-measurement. The observed net reaction proceeds according to the following equation [21]:

$$Zn^{2+} + H_2O \rightarrow ZnO + 2\ H^+$$

Hence, a simple method to determine the progress of this chemical reaction is to measure the time-dependent changes in the release of hydronium ions. In our case, we monitored the Trizma-buffered (pH = 8) reaction via titration of the gelatin-containing solution with nitric acid (40 mmol l^{-1}). The pH values were determind with a pH electrode for each temperature and were translated to time-depending supersaturation curves by using the titration curves as a conversion table. The supersaturation S is defined by $S = c/c_e$, where c is the concentration of zinc ions in the solution and c_e the corresponding equilibrium concentration.

3. RESULTS SECTION

3.1. Precipitation kinetics in absence of gelatin B 225. Diverse studies have characterized the precipitation of zinc oxide [21-23]. The occurrence of several phases including an amorphous phase, zinc hydroxide and crystalline zinc oxide during the precipitation process is mentioned [24-26]. As illustrated in figure 1a, all DLS curves start with an almost horizontal region which becomes more extended with decreasing temperature (40 min at 37 °C; 120 min at 30 °C; 400 min at 25 °C). The particle size in this period reaches values not larger than 30 nm, supported by the histogram in figure 1b. During this induction time of the reaction the particle size is in the range of the detection limit of the DLS technique [13]. XRD investigations of the precipitates observed during these periods give no evidence for crystallinity, which means, that the initial products of mineralization are amorphous (data not shown). After this period of time, the particles grow with a temperature-dependent growth rate and reach sizes up to several micrometers. In this growth section, the linear increase of the particle size was analyzed to gather kinetic data of particle growth. The kinetic evaluation of these data was done by calculating a rate constant [13], whose temperature dependence allows determining an apparent activation energy, following the Arrhenius equation (2):

$$k \sim \exp\left(\frac{-E_A}{RT}\right)$$

where k is the temperature-dependent rate constant, E_A is the molar activation energy, R is the ideal gas constant and T the absolute temperature [13,27].

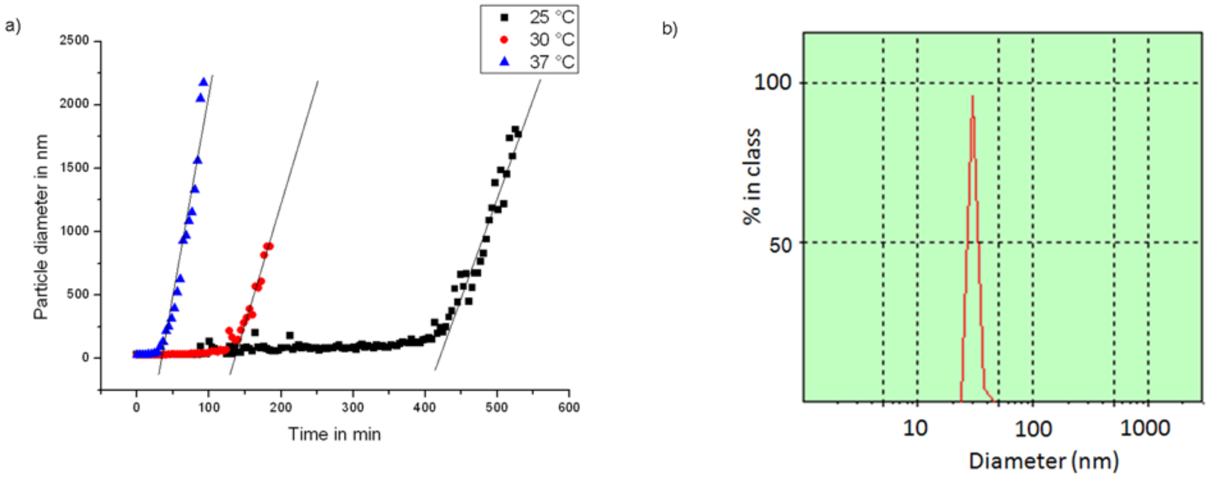

Figure 1: a) Precipitation of ZnO in absence of gelatin B 225. Particle size as measured by DLS vs. time at diverse temperatures. b) Histogram of the particle size as measured by DLS after 4 minutes in absence of gelatin B 225 at 25 °C.

In a first step, we determined the rate constants from the slope of the growth sector, as illustrated in figure 1a with the straight lines of the best fit. Afterwards, the temperature dependence of the growth rate allows us the determination of an activation energy of particle growth $E_{A,ZnO}$ by plotting the natural logarithm of the rate constant versus the reciprocal temperature. As shown in figure 2a, an activation energy of $E_{A,ZnO} = (71.0 \pm 10)$ kJ mol^{-1} has been obtained. The above mentioned assumptions were justified by the excellent linear correlation of $R^2 = 0.985$. The error bars for every data point were calculated from the standard deviation of the slope of each growth curve. In addition to the kinetics, the morphology of the particles was studied also. As observed by eye, sedimentation occurs in absence of gelatin B 225. SEM micrographs of the precipitated particles revealed spherical agglomerates consisting of primary particles of about 30 nm (figure 3). Corresponding XRD data reveal, that these particles consist of zinc oxide (JCPDS card no. 36-1451). The high activation energy $E_{A,ZnO}$ of (71.0 ± 10) kJ mol^{-1} is a hint for an agglomeration mechanism of the positively charged ZnO particles, which have an isoelectric point (pI) between 8.7 and 10.3 [28–30], within the Trizma-buffered solution (pH = 8). The described agglomeration process is supported by the fact, that particle size of about 30 nm is consistent with the primary particle size detected by DLS (cf. figure 1a).

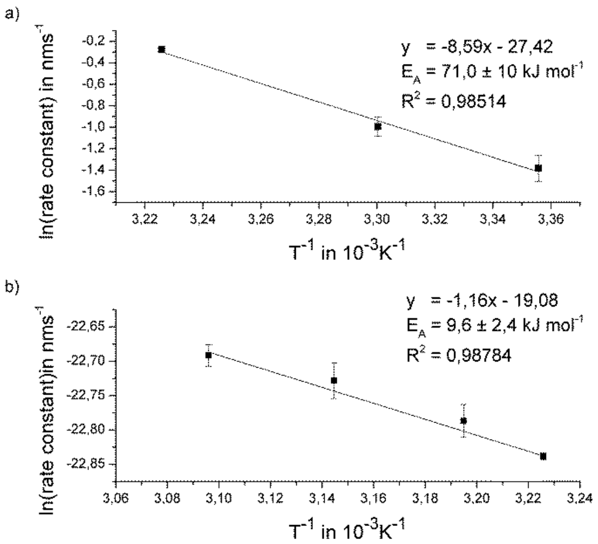

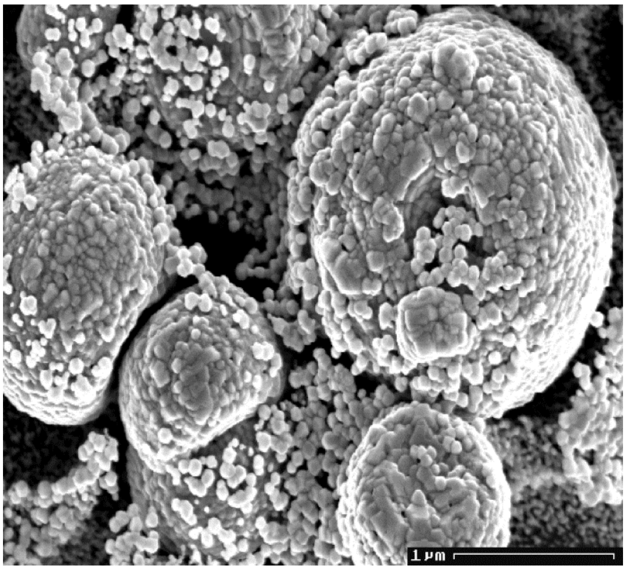

Figure 2: Arrhenius plots derived from DLS data. a) Particle growth in absence of gelatin B 225. b) Particle growth in presence of gelatin B 225.

Figure 3: Particles precipitated without gelatin B 225 at 37 °C after 100 minutes.

3.2. Precipitation kinetics in presence of gelatin B 225. In order to investigate the influence of gelatin B 225 on the precipitation process in detail, several investigations were done below and above the helix-coil transition temperature of gelatin B 225, which is found in literature below 40 °C [31]. Figure 4a shows the comparison of the particle growth (with and without the presence of gelatin B 225) at 30 °C and 37 °C, determined by DLS.

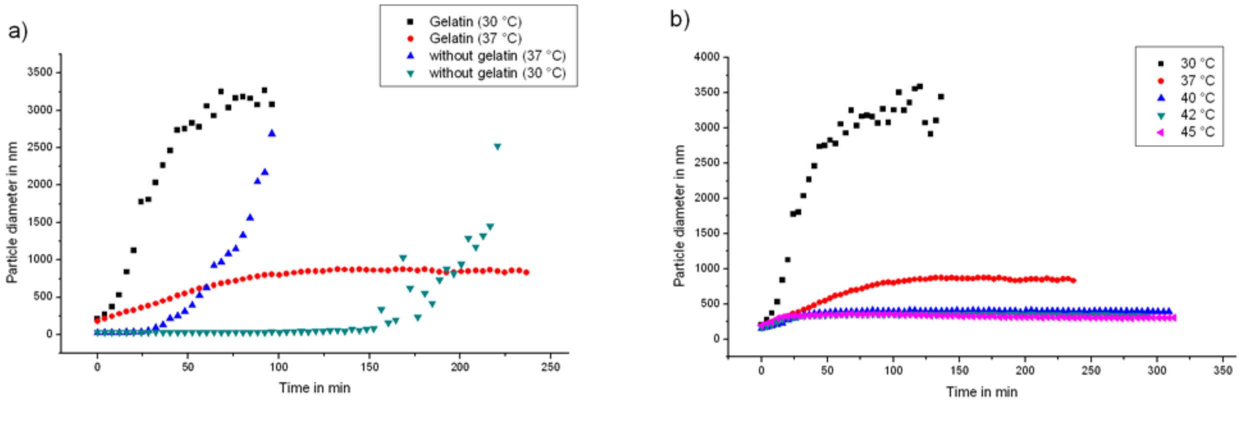

Figure 4: a) Particle size measurements. Precipitation with and without gelatin B 225; particle size as measured by DLS vs. time at 30 and 37 °C. b) Particle size measurements. Precipitation with gelatin B 225; particle size as measured by DLS vs. time at temperatures between 30 and 45 °C.

At 30 °C, the particles in solution with gelatin B 225 exhibit a high growth rate comparable to the one of those in solution without organic additive and reach sizes up to 3.5 µm. However, when the reaction temperature is increased to 37 °C, the particles grow slower and reach sizes only up to 0.8 µm. This difference in the growth rate by slightly change of the temperature can be correlated with the above mentioned helix-coil transition of gelatin B 225. This indicates, that the helix-coil transition leads to a modification of the mineralization behavior. Obviously the opening process of the helical conformation to the coil structure releases additional active centers for mineralization.

The strong scattering of the measured data at 30 °C after 60 min in figure 4a can be associated to the sedimentation of the particles, as proved via observation by eye.

Accordingly, temperatures above the helix-coil transition were selected and examined in more detail. Figure 4b shows the DLS course of the hydrodynamic diameter of precipitated particles obtained from reactions conducted at temperatures between 30 °C and 45 °C. In a first stage, the particles grow proportional to time, then their size trends to a certain value between ~900 nm at 37 °C and 250–400 nm at higher temperatures. As shown in figure 4b, the particle growth at 37 °C is noticeably located between the growths of 30 °C and higher temperatures, which is a hint that the helix-coil transition of gelatin B 225 is not fully completed at 37 °C. An incubation time as observed for the samples without gelatin B 225 cannot be detected. The missing of an incubation time is a hint, that the precipitation process is diffusion controlled, as reported in literature [32].

To evaluate the influence of the organic component, also the hydrodynamic diameter of gelatin B 225 was measured in the buffer solution at 37 °C by DLS. We found a size of $dH = (112 \pm 7.2)$ nm that is in the same order of magnitude as the size determined by Bohidar et al. [33] According to the Mie theory, the scattering intensity is proportional to the sixth power of the particle diameter [34]. Regarding the DLS curves in the figures 4a–b, therefore, it was not possible to detect precipitated particles in the range below ~120 nm.

The previously described results reveal that the particle growth of ZnO in absence of gelatin B 225 is definitely faster than in presence of gelatin B 225, which can be calculated from DLS data. At 37 °C the growth rate of ZnO particles is 45.6 nm min^{-1} in absence of gelatin B 225. In presence of gelatin B 225 the growth rate is only 7.2 nm min^{-1}. The corresponding Arrhenius plot from which the activation energy of growth in presence of gelatin $E_{A,g}$ was calculated, is illustrated in figure 2b. The activation energy derived from the slope of the linear correlation amounts to $E_{A,g} = 9.6 \pm 2{,}4$ kJ mol^{-1} ($R^2 = 0.987$). This is a drastic decrease in relation to the activation energy of growth in absence of gelatin $E_{A,ZnO}$ (71.0 ± 10 kJ mol^{-1}) and indicates that the particle interactions of the system are significantly influenced by gelatin B 225.

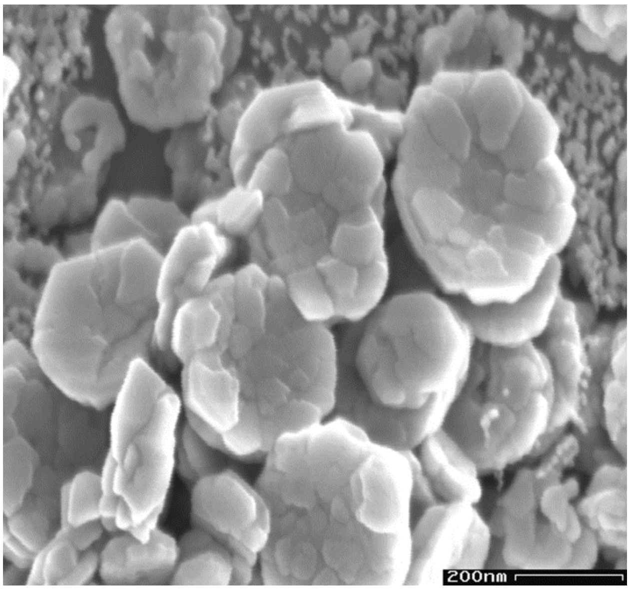

Figure 5: Hexagonal agglomerates formed at 45 °C after 100 minutes with gelatin B 225.

Table 1: Particle sizes in nm after a reaction time of 100 min with gelatin B 225, before (45 °C) and after heating up to 600 °C.

Reflex	before	after
(100)	15	37
(002)	8	25
(101)	11	33

The particle growth can be correlated with an agglomeration process. In this connection the activation energy of particle diffusion [33,35] in our system was determined. The agglomeration was revealed by the observation, that the precipitated particles are agglomerates consisting of individual zinc oxide crystals, as shown in figure 5, where the SEM micrograph of gelatin B 225 at 45 °C after 100 min and subsequent is exemplarily illustrated. Please note that the size of the individual zinc oxide crystals is increased by the factor 2.5-3 compared to the one observed for the as-received products due to the subsequent annealing step at 600 °C, which was necessary to remove the gelatin matrix and to reveal the particles (table 1). The small increase of only 2.5 along [100] is in accordance to the tendency, that zinc oxide forms rather elongated crystals along the [001] axis [36].

From the DLS measurements, the calculation of the activation energy of particle diffusion EA,d was realized according to equation 1. The calculated EA,d values are between 13.5 kJ mol^{-1} and 15.5 kJ mol^{-1}. Hence, the values of particle diffusion $E_{A,d}$ are in the order of magnitude of the above mentioned activation energy of growth $E_{A,g} = 9.6 \pm 2.4$ kJ mol^{-1}.

3.3. Stages of particle formation. The DLS observations in presence of gelatin B 225 suggest that for the processes in the solution three distinct stages of particle formation can be identified (cf. figure 4b): an initial stage, where the particles grow proportional to the time (growth state); a transition stage and a final stage, where the hydrodynamic diameter stays constant.

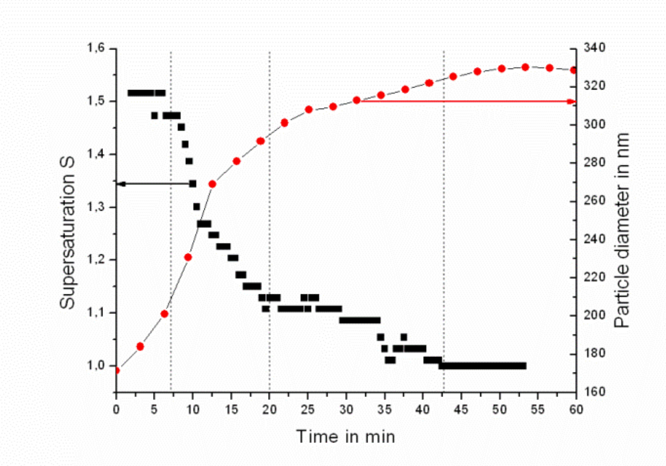

Figure 6: Supersaturation (black squares) and particle diameter (red dots) versus time at 45 °C with gelatin B 225.

In order to receive an overview about the precipitation process in these three stages in terms of the occurring phases, size and morphology of the particles, it is necessary to study the chronological sequence of particle formation. Figure 6 represents an exemplary overview about the evolution of supersaturation, which was obtained by measuring titration curves during time (see section pH measurement), and the particle size in presence of gelatin B 225 at 45 °C up to 60 min of the reaction time. Regarding the decay of the supersaturation curves the most drastic changes appear in the first 20 min, where the relative reaction rate steeply drops down. Within the final region after 43 min the supersaturation remains at a constant level of about 1. The drastic drop down of the supersaturation during the first 20 min can be interpreted is an effect of electrostatic interaction between gelatin B 225 and the ZnO-forming species in solution. In literature, values for the isoelectric point pI of gelatin type B between 3.5 and 6.5 are reported [37]. The pH of the reaction solution in our experiments is about 8. Therefore, the negatively charged gelatin B 225 is expected to interact with the positively charged zinc ions and precursor clusters, which is completely in accordance with the reactions described for peptides in zinc salt solutions [38].

To get further hints concerning the described mechanism, additional XRD measurements were made (figure 7): The XRD diffractogram of a sample let to react up to 25 minutes exhibits a broad peak at 2θ = 33°. It can be assigned to a metastable zinc hydroxide phase [25], which is formed first. During this time, reflections of zinc oxide crystals were not detectable with XRD. After this period, which corresponds to the first stage of particle formation discussed above (figure 6), XRD data revealed diffraction peaks assigned to crystalline ZnO (JCPDS card no. 36-1451). The corresponding SEM indicates the formation of hexagonal aggregates embedded in gelatin matrix, as shown in figure 8. The further chronological development observed on the XRD diffractograms of samples taken after longer reaction time (figure 7) can be interpreted according to Ostwald rule of stages as a dissolution-recrystallization mechanism, where zinc hydroxide transforms as an intermediate product into zinc oxide. This is in analogy to the basic mechanisms of biomineralization induced by organic templates also known from the literature [5,10,12,39,40].

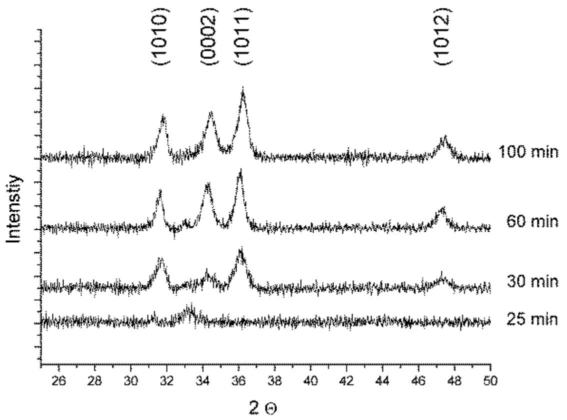

Figure 7: X-ray diffractograms of the material with gelatin B 225 at the reaction temperature of 45 °C before heating up to 600 °C in dependence of the reaction time. The peaks are indexed to zinc oxide according to JCPDS card no. 36-1451. The reflex at 2θ = 33.5° can be assigned to metastable zinc hydroxide

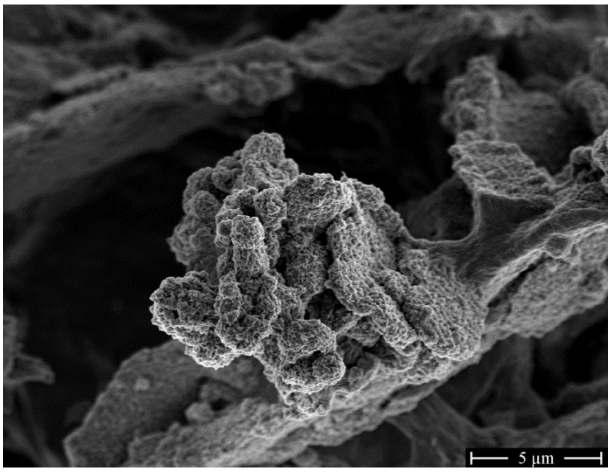

Figure 8: Hexagonal aggregates of ZnO embedded in gelatin matrix formed at 45 °C after 30 minutes.

In the final stage of after a reaction time of 100 min a stable particle is reached. It was proven that this stable particle size is caused by a ceasing mineralization due to the depletion of reaction solution with zinc. In experiments we confirmed this with repeated addition of the same amount of educts to the suspension at fixed periods of time (every 100 min) during the final stage. The existing particles grow further at these points. After that, again a constant particle size is detected (figure 9).

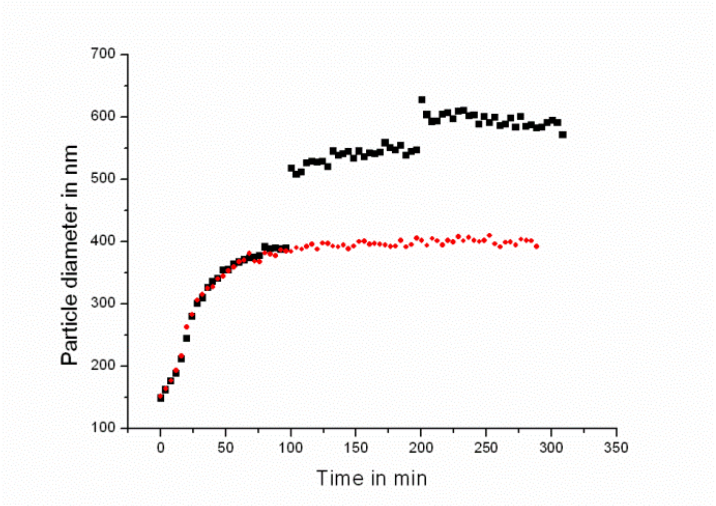

Figure 9: Development of particle size at 40 °C. After 100 min and 200 min, new educts were added (black squares). The development of particle size without adding new educts is also illustrated (red dots).

3.4. Mechanism. Based on these data, we propose the following mechanism: In the precipitation process without gelatin B 225, two stages can be distinguished. In the first step, amorphous nanoparticles with a size in the range of about 30 nm are formed during the incubation time and the particle size remains constant, as can be shown by in situ DLS measurements (figures 1 and 4a). Via a dissolution precipitation mechanism these intermediates then transform into zinc oxide nanoparticles, which agglomerate to spherical micro-sized particles (figure 3). The activation energy can be determined to be $E_A \approx 71$ kJ mol^{-1}. This relatively high value can be referred to the equal electrostatic positive charge of the agglomerating zinc oxide nanoparticles.

In presence of gelatin B 225, in situ DLS measurements indicate particle growths in the early stage. The negative charge of gelatin B 225 at this pH is crucial for the electrostatic attraction of the positively charged reaction species. During this early period, metastable zinc hydroxide is formed, as shown by XRD (figure 7). The calculated relatively low activation energy E_A of about 9.6 kJ mol^{-1} reflects the positive interaction between anionic gelatin and cationic species within the deposition solution. According to Ostwald rule of stages, the metastable intermediate transforms into the stable ZnO phase in the second stage, which has also be described in other systems [5,10,12,26]. The phase transformation to stable zinc oxide nanocrystals was shown by XRD data, by the appearance of the characteristic (100)-, (002)- and (101)-reflections of ZnO and the corresponding disappearance of the hydroxide phase (figure 7). The gelatin-controlled mineralization process finally yields hexagonally-shaped polycrystals. The size of these crystals can be increased by the further addition of zinc salt to the depleted reaction solution.

4. CONCLUSIONS

In this contribution, we investigated the precipitation process of zinc oxide, both in absence and presence of gelatin B 225. The presence of the organic additive, in our case gelatin B 225, has a strong influence on the mineralization process. In absence of gelatin, the precipitation process starts after an incubation time, the particles grow to spherical agglomerates of several microns and sedimentation occurs. In contrast to this behavior, the presence of gelatin B 225 effects the formation of hexagonal agglomerates of a few hundred nanometers and a particle growth without an incubation time.

In the stage of particle growth, kinetic analysis of the DLS data revealed that the activation energy of particle growth is lowered by gelatin from $E_{A,ZnO} = (71 \pm 10)$ kJ mol^{-1} in absence to $E_{A,g} = (9.6 \pm 2{,}4)$ kJ mol^{-1} in presence of gelatin. This can be attributed to attractive electrostatic interactions provided by the negatively charged bioorganic template and positively charged zinc ion-containing species in solution. In presence of gelatin, the activation energy of particle growth $E_{A,g}$ and the activation energy of particle diffusion $E_{A,d}$ are in the same order of magnitude. This suggests that the agglomeration process is limited by particle diffusion.

5. ACKNOWLEDGMENT

We are grateful for financial support provided by the DFG (BI 469/15-1) within the scope of the project “Biologische Erzeugung von Oxidkeramiken” (PAK 410). The authors gratefully acknowledge Natalia Egana and Felicitas Predel for technical support. Maritta Dudek (MPI-IS) is thanked for the XRD measurements. Prof. Dr. P. A. van Aken (MPI-IS) is thanked for providing the SEM.

6. REFERENCES

[1] Chopra K. L., Major S., Pandya D. K., Transparent conductors - A status report, *Thin Solid Films* 102, 1-46, **1983**

[2] Pearton S. J., Norton D. P., Ip K., Heo Y. W., Steiner T., Recent progress in processing and properties of ZnO, *Progress Mater Sci.* 50, 293-340, **2007**
[3] Leary D. J., Barnes J. O., Jordan A. G., Calculation of carrier concentration in polycrystalline films as a function of surface acceptor state density: application for ZnO gas sensors, *J. Electrochem. Soc.* 129, 1382-1386, **1982**
[4] Oh B. Y., Jeong M. C., Moon T. H., Lee W., Myoung J. M., Hwang J. Y., Seo D. S., Transparent conductive Al-doped ZnO films for liquid crystal displays, *J. Appl. Phys.* 99, 124505, **2006**
[5] Baeuerlein E., *Handbook of Biomineralization*, Wiley-VCH, **2007**
[6] Cölfen H., Antonietti M., *Mesocrystals and Nonclassical Crystallization,* Wiley, **2008**
[7] Bauermann L. P., Bill J., Aldinger F., Bio-friendly Synthesis of ZnO Nanoparticles in Aqueous Solution at Near-Neutral pH and Low Temperature, *J. Phys. Chem.* 110, 5182-5185, **2006**
[8] Bauermann L. P., del Campo A., Bill J., Aldinger F., Heterogeneous Nucleation of ZnO Using Gelatin as the Organic Matrix, *Chem. Mater.* 18, 2016-2020, **2006**
[9] Bauermann L. P., Bill J., Aldinger F., Bio-inspired syntheses of ZnO-protein composites, *Int. J. Mat. Res.* 98, 879-883, **2007**
[10] Cölfen H., Mann S., Higher-Order Organization by Mesoscale Self-Assembly and Transformation of Hybrid Nanostructures, *Angew. Chem. Int. Ed.* 42, 2350-2365, **2003**
[11] Andeen D., Kim J. H., Lange F. F., Goh, G. K. L., Tripathy, S., Lateral epitaxial overgrowth of ZnO in water at 90 °C, *Adv. Funct. Mater.* 16, 799-804, **2006**
[12] Lipowski P., Hedin N., Bill J., Hoffmann R. C., Ahniyaz A., Aldinger F., Bergström L., Controlling the Assembly of Nanocrystalline ZnO Films by a Transient Amorphous Phase in Solution, *J. Phys. Chem. C* 112, 5373-5383, **2008**
[13] Cölfen H., Schnablegger H., Fischer A., Jentoft F. C., Weinberg G., Schlögl R., Particle Growth Kinetics in Zirconium Sulfate Aqueous Solutions Followed by Dynamic Light Scattering and Analytical Ultracentrifugation: Implications for Thin Film Deposition, *Langmuir* 18, 3500-3509, **2002**
[14] Bishop J. B., Martin J. C., Rosenblum W. M., A light scattering method for qualitatively monitoring aggregation rates in macromolecular systems, *J. Crystal Growth* 110, 164-170, **1991**
[15] Georgalis Y., Schüler J., Frank J., Soumpasis M. D., Saenger W., Protein crystallization screening through scattering techniques, *Adv. Colloid and Interface Sci.* 58, 57-86, **1995**
[16] Juarez-Martinez G., Garza C., Castillo R., Moreno A., A dynamic light scattering investigation of the nucleation and growth of thaumatin crystals, *J. Crystal Growth*, 232, 119-131, **2001**
[17] Manual PCS theory, Malvern Instruments Zetasizer 3000HS Advanced
[18] da C. Andrade E. N., A theory of the viscosity of liquids. - Part I., *Philos. Mag.* 17, 497-511, **1934**
[19] Gorna K., Munoz-Espi R., Gröhn F., Wegner G., Bioinspired Mineralization of Inorganics from Aqueous Media Controlled by Synthetic Polymers, *Macromol. Biosci.* 7, 163-173, **2007**
[20] Mittemeijer E. J., Welzel U., The „state of the art“ of the diffractiob analysis of crystallite size and lattice strain, *Z. Kristall.* 223, 552-560, **2008**
[21] Schindler P., Althaus H., Feitknecht W., Löslichkeitsprodukte und Freie Bildungsenthalpien von Zinkoxid, amorphen Zinkhydroxid, β_1-, β_2-, γ-, δ- und ε-Zinkhydroxid, *Helvetica Chimica Acta* 47, 982-991, **1964**
[22] Schindler P., Althaus H., Hofer F., Minder W., Löslichkeitsprodukte von Zinkhydroxid, Kupferhydroxid und Kupferoxid, in abhängigkeit von Teilchengröße und molarer Oberfläche. Ein Beitrag zur Thermodynamik von Grenzflächen fest-flüssig, *Helvetica Chimica Acta* 48, 1204-1215, **1965**
[23] Bénézeth P., Palmer D. A., Wesolowski D. J., The solubility of zinc oxide in 0.03 m NaTr as a function of temperature, with in situ pH measurement, *Geochim. Cosmochim. Acta* 63, 1571-1586, **1999**
[24] Feitknecht W., Über das Altern gelförmiger basischer Zinksalze. Zur Kenntnis topochemischer Reaktionen kompaktdisperser Stoffe, *Kolloid-Z.* 68, 184-190, **1934**
[25] Feitknecht W., Häberli E., Über die Löslichkeitsprodukte einiger Hydroxyverbindungen des Zinks, *Helv. Chim. Acta* 124, 922-936, **1950**
[26] Lieth R. M. A., *Preparation and crystal growth of materials with layered structures,* Reidel Publishing Company, **1977**
[27] Flory P. J., Weaver E. S., Helix - Coil Transitions in Dilute Aqueous Collagen Solutions, *J. Am. Chem. Soc*. 82, 4518-4525, **1960**
[28] Parks G. A., The Isoelectric Points of Solid Oxides, Solid Hydroxides, and Aqueous Hydroxo Complex Systems, *Chem. Rev*. 65, 177-198, **1965**
[29] Degen A., Kosec, M., Effect of pH and impurities on the surface charge of zinc oxide in aqueous solution, *J. Europ. Ceramic Soc. 20*, 667-673, **2000**

[30] Salmang H., Scholze H., *Keramik,* Springer, **2007**

[31] Elysée-Collen B., Lencki R. W., Protein Ternary Phase Diagrams. 1. Effect of Ethanol, Ammonium Sulfate, and Temperature on the Phase Behavior of Type B Gelatin, *J. Agric. Food Chem*. 44, 1651-1657, **1996**

[32] Nielsen A. E., *Kinetics of precipitation,* Pergamon Press, **1964**

[33] Bohidar H. B., Hydrodynamic properties of gelatin in dilute solutions, *Int. J. Biol. Macromol.*, 23, 1-6, **1998**

[34] Mie G., Beiträge zur Optik trüber Medien, speziell kolloidaler Metallösungen, *Annalen der Physik* 330, 377-455, **1908**

[35] Smoluchowski M., Mathematical theory of the kinetics of the coagulation of colloidal solutions, *Z. Phys. Chem*. 92, 129-168, **1917**

[36] Andrés Vergés M., Mifsud A., Serna C. J., Formation of Rod-like Zinc Oxide Microcrystals in Homogeneous Solutions, *J. Chem. Soc. Faraday Trans.* 86, 959-963, **1990**

[37] ALFATEC-PHARMA GmbH, EP patent, EP 0 615 445 B1

[38] Gerstel P., Lipowsky P., Durupthy O., Hoffmann R. C., Bellina P., Bill J., Aldinger F., Depositopn of Zinc Oxide and Basic Zinc Salts from Aqueous Solutions Containing Amion Acids and Dipeptides, *J. Ceram. Soc. Japan* 114, 911-917, **2006**

[39] Mann S., Die Chemie der Form, *Angew. Chem*. 112, 3532-3548, **2000**

[40] Pouget E. M., Bomans P. H. H., Goos J. A. C. M., Frederik P. M., de With G., Sommerdijk N. A. J. M., The Initial Stages of Template-Controlled $CaCO_3$ Formation Revealed by Cryo-TEM, *Science* 323, 1455-1458, **2009**